REPORT DOCUMENTATION PAGE

AFRL-SR-BL-TR-01-

0317

1. AGENCY USE ONLY *(Leave blank)*	2. REPORT DATE	3. REPORT TYPE AND DATES COVERED
	18 Apr 01	FINAL REPORT 01 Oct 96 TO 30 Sep 99

4. TITLE AND SUBTITLE
DEVELOPMENT AND CALIBRATION OF WALL-SHEAR-STRESS MICROSENSOR SYSTEMS

5. FUNDING NUMBERS
F49620-96-1-0482

6. AUTHOR(S)
Eli Reshotko
Mehran Mehregany

7. PERFORMING ORGANIZATION NAME(S) AND ADDRESS(ES)
CASE WESTERN RESERVE UNIVERSITY
10900 Euclid Avenue
Cleveland, Ohio 44106-7222

8. PERFORMING ORGANIZATION REPORT NUMBER

9. SPONSORING/MONITORING AGENCY NAME(S) AND ADDRESS(ES)
AFOSR/NA
801 N. Randolph St.
Arlington VA 22203

20010508 054

11. SUPPLEMENTARY NOTES

12a. DISTRIBUTION AVAILABILITY STATEMENT

Cleared for public distribution

12b. DISTRIBUTION CODE

13. ABSTRACT *(Maximum 200 words)*

The long term objective of this program has been to develop the requisite technologies for integrating different sensors and actuators in desired combinations with electronics and telemetry on the same substrate. This has been a multi-year program. We are now completing the program

Our concentration has been on wall-shear-stress sensors. We have produced and calibrated floating element wall-shear-stress sensors, both active and passive. We have developed a calibration channel and a calibration procedure based on continuum isothermal compressible channel flow. We have also developed and tested a wall-shear-stress sensors with integrated electronics initially based on the Analog Devices Inc. (AD1) airbag accelerometer circuitry, and more recently on one developed at CWRU.

This most recent work continued the emphasis on the accuracy of the calibration process toward reducing the uncertainty of measurement from the past estimate of 5% to a goal of 1%. Our results are reported in a M.S Thesis recently completed, followed by some additional Navier-Stokes computations. A journal manuscript is in preparation.

14. SUBJECT TERMS
CALIBRATION OF WALL-SHEAR-STRESS MICROSENSOR SYSTEMS

15. NUMBER OF PAGES

16. PRICE CODE

17. SECURITY CLASSIFICATION OF REPORT	18. SECURITY CLASSIFICATION OF THIS PAGE	19. SECURITY CLASSIFICATION OF ABSTRACT	20. LIMITATION OF ABSTRACT
UNCLASSIFIED	UNCLASSIFIED	UNCLASSIFIED	UL

FINAL REPORT

DEVELOPMENT AND CALIBRATION OF WALL-SHEAR-STRESS MICROSENSOR SYSTEMS

AFOSR GRANT F49620-96-1-0482

Eli Reshotko

Department of Mechanical and Aerospace Engineering

Mehran Mehregany

Department of Electrical Engineering and Applied Physics

Case School of Engineering
Case Western Reserve University
Cleveland, Ohio

March 2001

Abstract
The long term objective of this program has been to develop the requisite technologies for integrating different sensors and actuators in desired combinations with electronics and telemetry on the same substrate. This has been a multi-year program. We are now completing the program

Our concentration has been on wall-shear-stress sensors. We have produced and calibrated floating element wall-shear-stress sensors, both active and passive. We have developed a calibration channel and a calibration procedure based on continuum isothermal compressible channel flow. We have also developed and tested a wall-shear-stress sensors with integrated electronics initially based on the Analog Devices Inc. (ADI) airbag accelerometer circuitry, and more recently on one developed at CWRU.

This most recent work continued the emphasis on the accuracy of the calibration process toward reducing the uncertainty of measurement from the past estimate of 5% to a goal of 1%. Our results are reported in a M.S Thesis recently completed, followed by some additional Navier-Stokes computations. A journal manuscript is in preparation.

Past Work
Prior to the start of this grant, we built a new calibration channel satisfying the requirements for non-leakage, non-choking, and having appropriate pressure and temperature measurements. The pressure measurements are required to evaluate the shear stress and the temperature measurements are to assure the isothermal character of the flow. It has been shown in our past work that in order to separate shear forces on the sensor element from pressure forces on the edge of the element, it is necessary to know the pressure gradient in the flow at the sensor location both during calibration and in operation.

Recent Work
1. Improving accuracy of the calibration process
In an effort to improve the accuracy and reduce the uncertainty in the calibration process, each element of the procedure was investigated in detail. The basic calibration relationship is

$$\tau = -(b/2)(dp/dx)(1-\gamma M^2)$$

where b is the height of the channel, dp/dx is the measured pressure gradient at the sensor location, γ is the ratio of specific heats of the test gas (nitrogen) and M is the Mach number at the sensor location. We have had our rotameters recalibrated by the manufacturer so that our Mach number determination is within 1%. The pressure measuring circuits have been cleaned out and now give reliable readings. Since it is the pressure *gradient* that is required, the absolute value of pressure is of lesser importance, but we are trying to get an independent verification of the pressure transducer calibration.

The largest inaccuracy is in the measurement of the channel height, *b*. Since this height is if the order of 200 μm, it is not measurable within 1% by any standard means. It is difficult to bring a microscope to the channel or vice-versa.

We have instead used the microwave technique called "Microstrip" (Pozar, David M.: Microwave Engineering, 2nd Ed., Wiley, 1998, pp.160 ff). A gold microstrip line is printed on the glass cover plate of the channel. The metal bottom of the channel is grounded. The transmission frequency that minimizes the reflected signal is directly related to the gap between the glass and the metal. Our measurements indicate a sensitivity of about ± 3μm which is about ±1.5% for a channel height of 200 μm. We believe our overall uncertainty now to be about ± 2%.

These results are presented in the M.S. Thesis of Mr. Mehul Patel entitled "Development of MEMS Wall Shear Stress Calibration System." A copy of the draft of a journal article based on this work is enclosed.

2. Navier-Stokes study of flow around the sensor element

The calibration relations used to date assume that the flow about the sensor element is subject to the same pressure gradient as in the center of the calibration channel. These assumptions were examined this past year in an unsponsored work by a M.S. student, Ms. Yng-Ru Chen. A presentation of this work is planned for the APS/DFD Annual Meeting in November 2001.

A two-dimensional commercially-available two-dimensional, incompressible Navier-Stokes code was applied to this problem. The flow domain included the full channel height plus the flow around and beneath the sensor element and extended from about one channel-height upstream – to about a channel-height downstream of the sensor element. The incoming flow in the main channel was assumed to be fully developed laminar channel flow at a Reynolds number of 600. Extra grid was concentrated in all the passages around and below the sensor element.

The results show that the pressure gradient on the channel side of the sensor element was essentially that in the free stream. Below the sensor element, the pressure gradient was less than in the free-stream by the amount of the pressure losses in the entrance and exit passages to the channel underneath the element. The flow beneath the sensor element displayed a parabolic profile of the appropriate speed to the pressure gradient and channel height. Because the channel height beneath the sensor element was 0.01 time the basic channel height, the Reynolds number beneath the sensor element is about 0.0006. The fron and rear edge surfaces of the sensor element displayed very unusual pressure distributions corresponding to the very low Reynolds number flow about them. The average pressure on the upstream edge was higher than in the free stream immediately above that edge, while the average pressure on the downstream edge was correspondingly lower than in the immediately above free stream. An analysis of these results shows that use of the assumed calibration relation systematically overestimates the surface shear stress by about 0.9%. This factor has to be introduced into the calibration process.

Also to be noted is that the flow in the passages around and below the sensor element are symmetric, as expected for this very low Reynolds number flow.

Personnel

The work on this grant over its entire period has been carried out by Messrs. Tao Pan, Daniel Hyman and Mehul Patel under the supervision of Profs. Reshotko and Mehregany with special assistance on electronic circuits from Prof. S. Garverick .

Honors and Awards

Dr. Reshotko received the 1999 Otto Laporte Award for Research in Fluid Dynamics, American Physical Society, "For lasting contributions and leadership to the understanding of transition to turbulence in high-speed flows and non-homogeneous flows."

Acknowledgement/Disclaimer

This work was sponsored (in part) by the Air Force Office of Scientific Research, USAF, under grant number F49620-96-1-0482. The views and conclusions contained herein are those of the authors and should not be interpreted as necessarily representing the official policies or endorsements, either expressed or implied, of the Air Force Office of Scientific Research or the U.S. Government.

Publications and Presentations over the period of this grant

Mehregany, M., DeAnna, R.G. and Reshotko, E.: "Microelectromechanical Systems for Aerodynamics Applications," AIAA Paper 96-0421, Jan. 1996

Reshotko, E., Pan, T. Hyman, D. and Mehregany, M.: "Characterization of Microfabricated Shear Stress Sensors," Eighth Beer-Sheva International Seminar on MHD Flows and Turbulence, Jerusalem, Israel, Feb. 1996

Reshotko, E., Mehregany, M. and Bang, C.: "MEMS Applications in Aerodynamic Measurement Technology,": AGARD-CP-601, May 1998, pp. 35-1 to 35-10. (Invited paper presented at RTO/AGARD FDP Symposium on Advanced Aerodynamic Measurement Technology, Seattle, Sept. 1997)

Reshotko, E., Pan, T., Hyman, D. and Mehregany, M.: "Characterization of Microfabricated Shear Stress Sensors," in H. Branover and Y. Unger, eds. *Progress in Fluid Flow Research: Turbulence and Applied MHD,* Progress in Aeronautics and Astronautics, vol. 182, chapt. 22, AIAA, 1998, pp.335-351

Pan, T., Hyman, D., Mehregany, M., Reshotko, E. and Garverick, S.: "Microfabricated Shear Stress Sensors, Part I: Design and Fabrication," AIAA Journal, vol. 37, no.1, Jan.1999, pp.66-72

Hyman, D., Pan, T., Reshotko, E. and Mehregany, M.: "Microfabricated Shear Stress Sensors, Part II: Testing and Calibration," AIAA Journal, vol. 37, no. 1, Jan. 1999, pp.73-78

Patel, Mehul: "Development of MEMS Wall Shear Stress Calibration System," M.S. Thesis, Department of Mechanical & Aerospace Engineering, Case Western Reserve University, May 2000

Development of MEMS Wall Shear Stress Calibration System

Mehul P. Patel* and Eli Reshotko†

Case Western Reserve University, Cleveland, Ohio 44106

A new calibration procedure for the development of wall shear stress sensors based on continuum isothermal compressible flow has been developed. The calibration relation is derived from the momentum theorem of fluid mechanics. Microelectromechanical based floating element sensors for direct measurement of wall shear stress are chosen for calibration. The calibration equation states a linear relation between the channel height and the calibrated shear stress, resulting in an overall calibration uncertainty derivative of measurement inaccuracy from the channel height. A novel microstrip technique formulated from the basic principles of microwave engineering has been applied to measure the channel height with an increased level of accuracy. The uncertainties involved in the measurement of all the parameters that are related in any way to the calibration equation are identified, measured, weighed and integrated into the equation to obtain a complete error

---

* Graduate Research Assistant, Department of Mechanical and Aerospace Engineering; currently Aerodynamics Engineer, Orbital Research Inc., 673 G Alpha drive, Cleveland, OH 44143.

† Kent H. Smith Professor of Engineering, Department of Mechanical and Aerospace Engineering, Fellow AIAA.

analysis of the calibration procedure. The calibration of shear stress sensors is successfully completed with an overall accuracy of 2%.

I. INTRODUCTION

The study of drag caused by a fluid flow over bodies of varied shapes is of vital importance to aerodynamic and hydrodynamic design. Knowledge of skin friction is of paramount importance, because friction determines a major part of the drag and can be an important factor in limiting or affecting the performance of a vehicle or structure. Wall shear stress is a quantity that is generally inferred since it cannot be easily measured. Despite the considerable work done on measurement of wall shear stress, there is still a need for an easily implementable and reliable technique of direct measurement of wall shear stress.[1, 2, 3, 4] The indirect techniques work under assumptions that relate the shear stress to the quantities that are directly measured. The only direct measurement technique is the floating-element technique, which use floating elements that displace against spring suspension systems when exposed to shear stress. Previous work describes the design, fabrication, testing and calibration of shear stress sensors based on the floating-element method with an overall inaccuracy of 5%.[5, 6, 7, 8] A flow channel that could sustain a two-dimensional continuum flow of nitrogen gas was designed for the calibration of Microelectromechancal systems (MEMS) sensors. An expected linear relationship between sensor deflection and shear stress was demonstrated and correlated with mechanical modeling.

This paper presents the refinement in the development of wall shear stress calibration system based on continuum isothermal compressible flow theory.[9] Flow channel is calibrated prior to the actual calibration of MEMS shear stress sensors. A novel micro-

strip technique based on the principles of microwave engineering is formulated to reduce the largest sources of error identified from channel height measurements. Finally, a complete error analysis of the calibration procedure has been carried out and integrated into the calibration equation.

II. MEMS Wall Shear Stress Sensors

The sensors used for calibration in the presented work are designed and fabricated using MEMS techniques. The floating element design on the MEMS shear stress sensors are based on a lateral resonant structure, a design that has been used in a number of microsensing and microactuating devices.[10, 11, 12] Lateral resonant structure features and theory are detailed in Ref. 7. A square floating element with tether suspension beams are microfabricated in polysilicon. Located at the center of the device, the floating element is suspended 2.5 microns above the lower electrodes by the folded beam suspension. The deflection of the folded suspension beam with applied shear force is linear. A picture of a MEMS sensor developed at Case Western Reserve University (CWRU) and Advanced MicroMachines for Industry (AMMI) used for calibration is shown in Fig. 1. The sensors use floating elements that displace against spring suspension systems when exposed to shear forces, thus qualifying as a direct measurement technique.

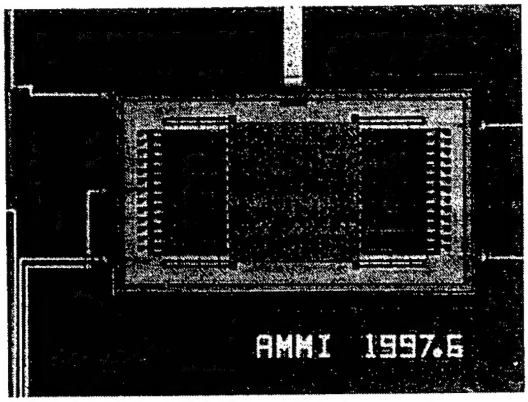

Fig. 1 CWRU/AMMI floating element shear stress sensor.

The application of MEMS technologies to fluid mechanics offers new possibilities for improved understanding of the physics of wall boundary layers.[13, 14, 15] In order to perform a complete analysis of wall shear stress, fluctuations occurring even in the mi-

cro scale (small eddies) have to be resolved. The scales of motion in a turbulent boundary layer are of the order of few hundred microns and the scale of the smallest eddies is about 100μm while the lifetime of these structures of the turbulent boundary layers is in milliseconds.[16] The sensor dimensions thus, needs to be smaller than the size of the smallest eddies. The most important features for a sensor that is used for measuring small-scale shear stress fluctuations, are small active sensor area and fast response time. Using micro-machined shear stress sensors, high spatial and temporal resolution can be obtained for the measurement of wall shear stress. Arrays of such sensors would allow the accurate mapping and analysis of turbulent structures, with speeds sufficient to detail their formation and destruction.

III. Theoretical Analysis

The schematic of the flow channel, which is used for sensor calibration, is shown in Fig. 2. The flow inside the high aspect ratio (96~145) continuum flow channel is approximated to be a two-dimensional flow. A steady continuous flow of nitrogen gas is supplied from a regulated nitrogen cylinder. For the channel with uniform cross sectional area, it is assumed that the pressure variation is only along the flow direction. The momentum theorem of fluid mechanics is used to derive the relation that is used for the calibration of the shear stress sensors,

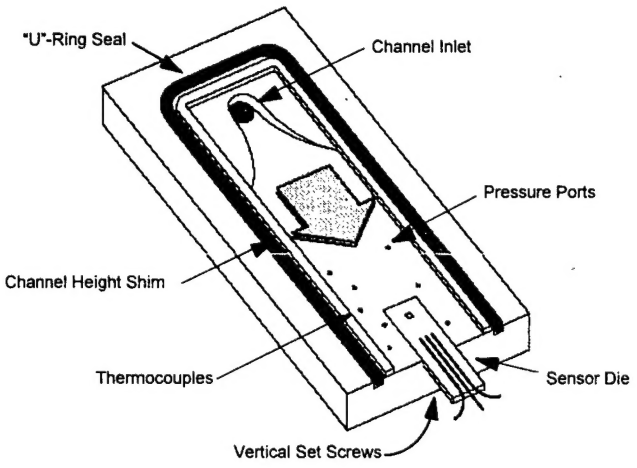

Fig. 2 Schematic of the flow channel base, shim and U-ring.

which makes the relation independent of whether the flow is laminar, transitional or turbulent.

Assumptions for the fluid flow are:

1. The flow is steady.

2. The local velocity or Mach number distributions can be represented by their mean values across the channel height.
3. Temperature is constant.

A control volume defined as an imaginary fixed volume through which, a fluid may flow is shown in Fig. 3. The pressure gradient inside the flow channel is the driving force of the fluid.

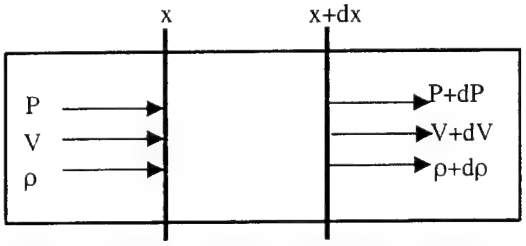

Fig. 3 Control volume of the flow channel.

A. Continuity Equation

The continuity equation states that

$$\rho AV = \text{constant} \qquad (1)$$

For an ideal gas, $p = \rho RT$ and $V = Ma$, where, $a = \sqrt{\gamma RT}$, Therefore (1) implies,

$$\frac{p}{RT} AM\sqrt{\gamma RT} = \text{constant} \qquad (2)$$

In differential form (2) becomes,

$$-\frac{1}{2}\frac{dT}{T} + \frac{dp}{p} + \frac{dA}{A} + \frac{1}{2}\frac{dM^2}{M^2} = 0$$

Since cross-sectional area is constant and gas is assumed to be isothermal, i.e. $\frac{dA}{A} = \frac{dT}{T} = 0$,

$$\text{Therefore, } dM^2 = -2M^2\frac{dp}{p} \qquad (3)$$

B. Momentum Balance

Applying momentum balance on a rigid control volume of differential size, we get:

$$\left[\rho V^2 \times b \times w\right]_{x+dx} - \left[\rho V^2 \times b \times w\right]_x =$$

$$\left[p \times b \times w - (p+dp) \times b \times w\right] - 2\tau_w w dx$$

$$\therefore \tau_w = \frac{b}{2}\left[-\frac{d}{dx}\left(\rho V^2\right) - \frac{dp}{dx}\right]$$

$$= -\frac{b}{2}\left[\frac{dp}{dx} + \frac{d}{dx}\left(\rho V^2\right)\right]$$

$$= -\frac{b}{2}\left[\frac{dp}{dx} + \frac{d}{dx}\left(\frac{p}{RT} M^2 \gamma RT\right)\right]$$

$$= -\frac{b}{2}\left[\frac{dp}{dx} + \frac{d}{dx}\left(p\gamma M^2\right)\right]$$

$$\Rightarrow \tau_w = -\frac{b}{2}\left[\frac{dp}{dx} + \gamma M^2 \frac{dp}{dx} + \gamma p \frac{dM^2}{dx}\right] \quad (4)$$

From (3),

$$\gamma p \frac{dM^2}{dx} = -2\gamma M^2 \frac{dp}{dx} \quad (5)$$

Substituting (5) in (4),

$$\tau_w = -\frac{b}{2}\left[\frac{dp}{dx}\left(1 - \gamma M^2\right)\right] \quad (6)$$

where, b is the channel height, τ_w is the wall shear stress and $\frac{dp}{dx}$ is the pressure gradient at the sensor location. The Mach number correction term in (6) incorporates the compressibility effect for an isothermal channel flow in the calibration equation.

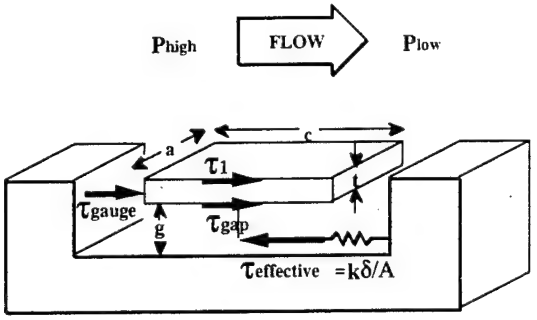

Fig. 4 Effective stresses on floating element.

There are other forces acting on the floating element, which are also considered for calculating the shear stress on the element. Fig. 4 shows the details of the floating element within the bed. The pressure gradient generated inside the flow channel is the driving force of the fluid. A "gauge thickness factor" as shown in Fig. 4 arises due to the pressure differential across the element, which forces the element to deflect in the

direction of the lower pressure. This additional gauge force is acting on the floating element and needs to be subtracted in order to accurately determine the wall shear stress.

F_{gauge}, can be measured as a pressure differential, ΔP_{gauge}, on the fore and the aft edge surfaces of the element. Let the dimensions t and a, be the thickness and the width normal to the page, respectively. The gauge factor F_{gauge}, can then be written as,

$$F_{gauge} = \Delta P_{gauge}\,(ta)$$

Let 'c' be the length of the floating element. The gauge pressure difference ΔP_{gauge}, is the pressure differential acting across the length c of the element and is equal to $\left(-c\frac{dp}{dx}\right)$. Therefore,

$$F_{gauge} = (ta)(-c\frac{dp}{dx})$$

The effective gauge stress τ_{gauge}, is then calculated by dividing the forces acting on the floating element by the top surface area of the element 'ac':

$$\tau_{gauge} = -t\frac{dp}{dx} \qquad (7)$$

Additionally, there is a small quantity of fluid flow underneath the floating element that contributes to yet another shear stress on the lower surface of the floating element, which is comparable to the gauge stress but very small compared to the top surface shear stress. Let 'g' be the gap spacing between the floating element and the fixed substrate. Then this shear stress is expressed as,

$$\tau_{gap} = -\frac{g}{2}\frac{dp}{dx} \qquad (8)$$

The effective applied shear stress after completing the force balance equation in the steady state can be written as,

$$\tau_{eff} = \tau_{w} + \tau_{gauge} + \tau_{gap}$$

(6), (7) and (8) give:

$$\tau_{eff} = -\frac{dp}{dx}\left|\frac{b}{2}\left(1-\gamma M^2\right)+\frac{g}{2}+t\right| \qquad (9)$$

The above equation shows the total applied force acting on the floating element divided by the upper surface area of the element during the actual calibration of the sensor. The shear stress on the working surface of the floating element, τ_w, is given by

$$\tau_w = \tau_{eff} - \tau_{gage} - \tau_{gap} = \tau_{eff} + \frac{dp}{dx}\left(\frac{g}{2}+t\right) \qquad (10)$$

IV. Calibration Apparatus

The use of a floating element sensor to measure τ_w requires a simultaneous measurement of the local pressure gradient. Sensor calibration involves the critical job of relating the sensor output to a primary shear stress standard. The two-dimensional isothermal compressible constant-area channel flow is regarded as such a standard.

A. The Flow Channel

A three-dimensional schematic of the assembled flow channel is shown in Fig. 2. The channel consists of a base plate made of stainless steel, a glass cover plate and a plastic shim. The thin plastic shim that defines the height and width of the channel is placed on the top of the base plate. The assembled flow channel is formed by clamping the glass cover plate over the shim with the help of another steel plate bolted with the bottom. The channel height can be varied by using shims of different thicknesses or by tightening and loosening the top screws. The channel height is varied to provide different ranges of wall shear stress at the sensor location inside the channel for the given flow rates. A U-ring is mounted outside the shim to provide a seal against side leakage. The assumption of a two-dimensional continuum fluid flow holds good due to the high aspect

ratio of the channel. Additional detail on the flow channel design is discussed in Ref. 8.

The micro-fabricated shear stress sensor, mounted on a microchip, is placed at a distance of 16.94 mm from the channel exit and is made flush with the channel bed by inserting it inside a machined groove. The groove dimension is such that it enables the top surface of the chip to fall in the same plane as the channel bed.

There are leveling screws as seen in Fig. 5 underneath the mounting plate of the sensor chip for very fine adjustments to make the sensor surface flush with the channel bed. A groove with a depth of 0.068 inches, which is standard for $1/8^{th}$ inch O-ring static seals, is machined into the base to accommodate a U-ring for separating the glass from metal and obtaining a leakage free flow channel. **Fig. 6** shows the location of the U-ring in preventing the leakage from the channel.

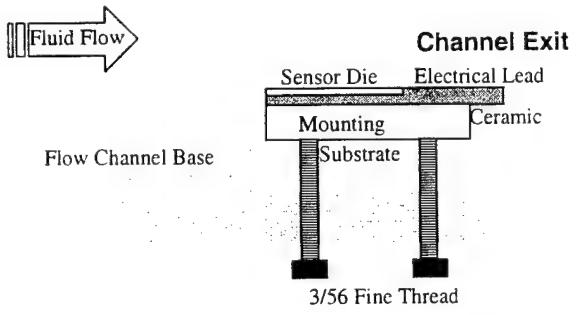

Fig. 5 Schematic of sensor mounting apparatus.

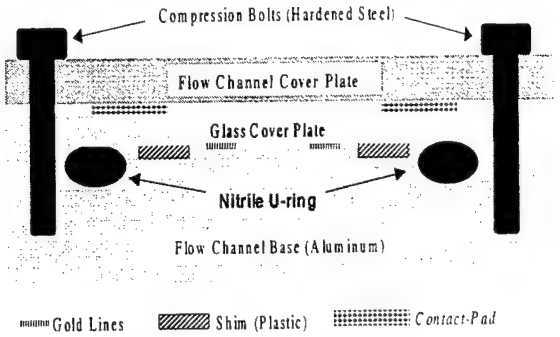

Fig. 6 Front view of the channel

B. PRESSURE TRANSDUCER

There are five miniature pressure taps that are drilled inside the channel. One end of each tap opens inside the channel and the other end of the taps are attached to different hoses, which are connected to a NIST calibrated pressure transducer OMEGA® PX236. The first pressure tap is located at a distance of 38.735mm from the channel end and the fifth tap is at a distance of 8.25mm from the channel end. A fixed distance of 7.625mm is maintained between each of the

taps to ensure uniformity. These taps enable direct measurement of the static pressures at these locations. A second order polynomial curve fit is made once the pressure readings at these five known locations are taken. The pressure gradient is obtained from differentiating this curve fit. The pressure at the sensor location is obtained by interpolation in the pressure distribution.

C. THERMOCOUPLES

Continuous monitoring of the temperature at different locations inside the flow channel is necessary to ensure isothermal conditions inside the channel. For this reason three tungsten wires acting as P-type thermocouples have been inserted in $1/16^{th}$ of an inch diameter holes at three different locations inside the channel bed from the bottom through drilled holes. The locations of these probes are at distances of 8.25 mm, 23.49 mm and 38.735 mm respectively from the channel end. The thermocouple tips are exposed to the inside of the channel. The thermocouple probes are inserted in such a manner that they provide a real time temperature measurement at all three locations without causing any obstruction to the fluid flow.

D. ROTAMETER

It is necessary to maintain a continuous non-fluctuating fluid flow for the calibration of the sensor. The rotameter controls and measures the flow rate that is required to calculate the Mach number of the fluid flow, which is eventually required for the calibration of the shear stress sensors. Two rotameters of different ranges of flow rates, certified with NIST calibration standards, are used in the experiment.

1. Low flowrate: 288.0-7590.0 (std ml/min)
2. High flowrate: 1384.6-46132.7 (std ml/min)

Both rotameters are certified with NIST calibration to ensure their accuracy.

V. Floating Element Shear Stress Micro-sensor with Differential Capacitive Read-out Scheme

A differential capacitive read-out scheme has been adopted to measure the position change of the floating element. When subjected to fluid flow, the shear force displaces the floating element, causing the element electrodes to move closer to one set of fixed electrodes and away from another. The two capacitances formed by the movable and fixed electrodes change accordingly; C_1 increasing and C_2 decreasing are then converted to voltages and amplified. On chip circuitry on the sensor chip provides force-balance sensor operation.[17, 18] Floating element voltage signal is modulated by an external referenced oscillator and fed into a preamplifier. This signal is fed back to the stationary electrodes as a bias signal. This bias incites an electrostatic force to attract the floating element towards the far electrode and away from the near electrode. Electrostatic forces in these devices are attractive only, such that the net attractive force in a given direction of interest causes the floating element to move back to its zero displacement position. Details of the differential capacitive read-out scheme for MEMS shear stress sensors used in this work are presented in Ref. 8.

VI. Measurement of Parameters

The parameters that need to be measured experimentally for shear stress determination from the calibration relation (9) are:

1. Channel height 'b', as defined by the thin shim thickness
2. Pressure gradient $\left(\frac{dp}{dx}\right)$, at the sensor location
3. Mach number 'M', at the sensor location
4. Thickness 't' of the floating element and
5. The gap 'g' between the floating element and the electrostatic shield.

A. CHANNEL HEIGHT

In the series of experiments that were performed for the calibration, the channel heights ranged from 180μm to 260μm. The height is varied depending on the dynamic range of the shear stress sensors that are used for calibration. Since, a linear dependency between channel height and shear stress exists in the calibration relation as shown in (9), the percent error in the measurement of channel height will contribute the same percentage error in the calculation of shear stress. Consequently, channel height b, the most difficult parameter to measure amongst all five parameters, is also the most important one. In the previous calibration technique, the channel height was measured using an optical microscope. The uncertainty in the measurement of the height with the optical measurement technique was estimated to be ±20μm. In the present work, a novel micro-strip technique has been designed from the fundamental principles of microwave engineering and has been demonstrated to reduce uncertainty in the measurement of channel height.

A1. MICRO-STRIPS

Micro-strip lines are thin planar transmission lines, which support electromagnetic waves at microwave frequencies. These lines are fabricated by photolithographic processes, in which conductive materials like gold or copper are deposited on a substrate. The geometry of such a micro-strip line is shown below. A conductor of width w is printed on a thin, grounded dielectric substrate of thickness d and relative permittivity ε_r. A sketch of the field lines is shown in Fig. 7.

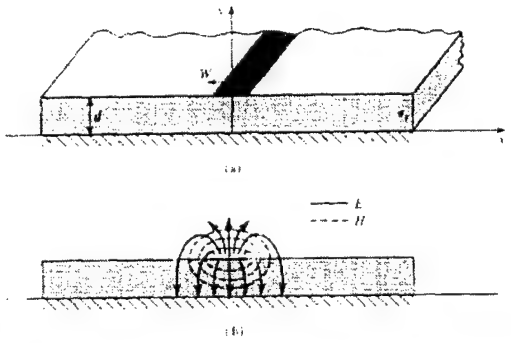

Fig. 7 Microstrip transmission line. (a) Geometry. (b) Electric and Magnetic field lines.[19]

Using a quasi-static approach, the phase velocity v_p and propagation constant β can be approximated as,

$$\text{Phase velocity, } v_p = \frac{c}{\sqrt{\varepsilon_e}}$$

$$\text{Propagation constant, } \beta = k_0\sqrt{\varepsilon_e},$$

where, $c = 3\times10^8$ m/sec is the speed of light and ε_e is the effective dielectric constant of the micro-strip line. For a lossless line, the characteristic impedance Z_0, which is the ratio of voltage to current for the traveling wave, is expressed as, $Z_0 = \sqrt{\frac{L}{C}}$, where L and C are inductance and capacitance per unit length of the line. Given the substrate (air) thickness, b, and conductor width, w, the characteristic impedance of the line, Z_0, is

$$Z_o = \frac{120\pi}{\sqrt{\varepsilon_e}\left[w/b + 1.393 + 0.667\ln\left(w/b + 1.444\right)\right]}$$

for $w/b \geq 1$ (11)

The 'w/d' ratio is given by

$$\frac{w}{b} = \frac{2}{\pi}\left[B - 1 - \ln(2B-1) + \frac{\varepsilon_e - 1}{2\varepsilon_e}\left\{\ln(B-1) + 0.39 - \frac{0.61}{\varepsilon_e}\right\}\right]$$

for $w/b \geq 2$ (12)

$$\text{Where, } B = \frac{377\pi}{2Z_0\sqrt{\varepsilon_e}}$$

A2. Design of the Gold Line

A gold line of width w and length l, as shown in Fig. 8, is deposited on the lower surface of the glass cover plate by a shadow mask process.[20, 21] The shim that separates the glass cover plate from the steel base plate defines the channel height b. The medium between the plates is air. The effective dielectric constant of air, ε_e, is 1. Now, if the characteristic impedance, Z_0, and width

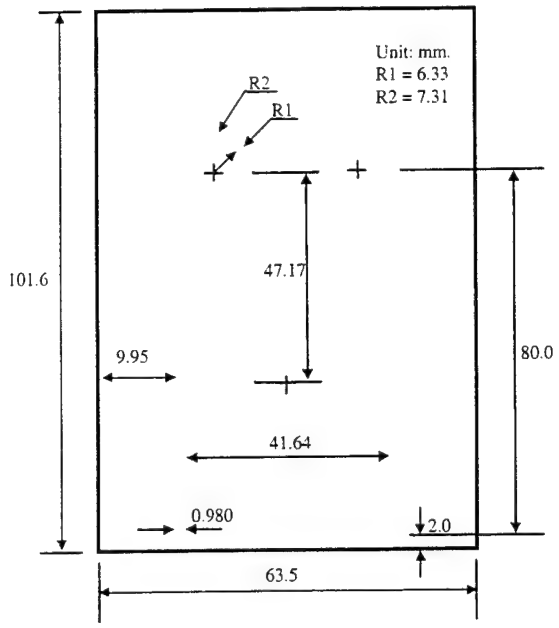

Fig. 8 The length of the transmission line.

w are fixed, the distance, b can be calculated from (11) and (12).

In the present design, an electromagnetic RF wave from a source inside the Network Analyzer-HP4395A is sent down the gold line. The characteristic impedance of the transmission line is 50Ω. The purpose of fixing the characteristic impedance to 50Ω is because of its standard usage in all types of applications. Fig. 9 is the block diagram of the set up for the channel height measurement. Fig. 10 is the analogy diagram to simplify and deduce the fact that the present design is no different than the actual application after taking into effect the effective permittivity of the glass and air.

(11) and (12) show that the interaction of the micro-strip with the conducting plane is extremely sensitive to their separation dis-

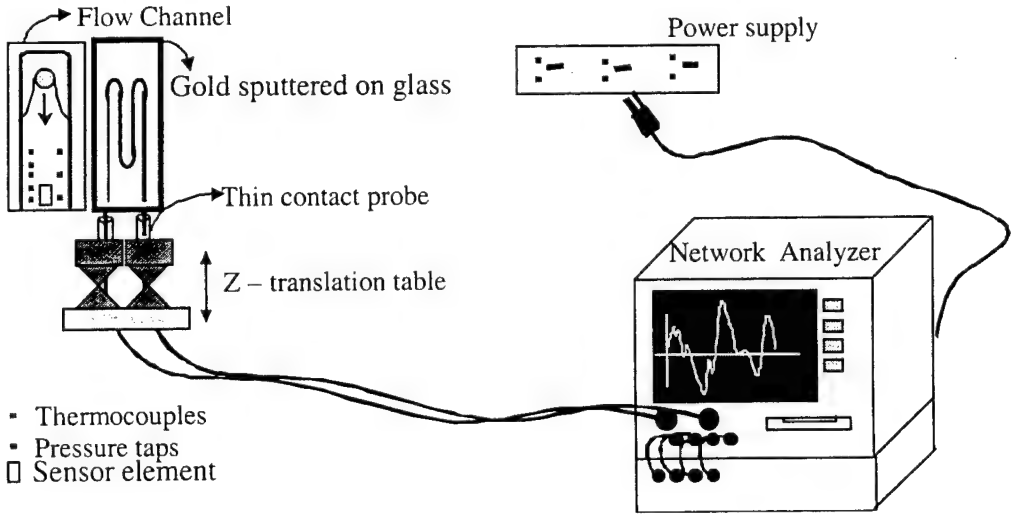

Fig. 9 Channel height measurement setup using HP4395A – Network Analyzer.

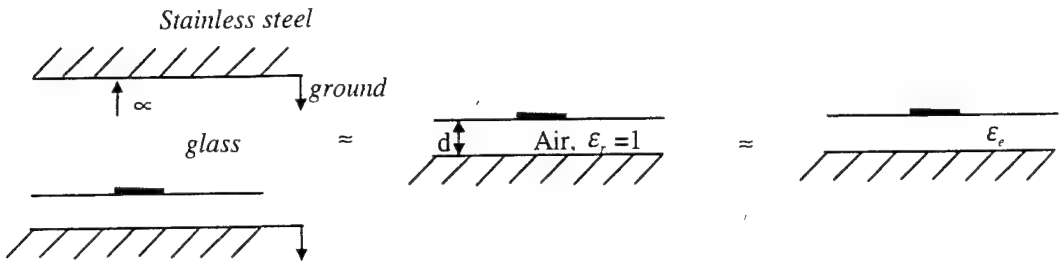

Fig. 10 Microstrip application - channel height measurement analogy diagram.

tance (channel height). The channel base is treated as an infinite conducting plane some distance away from the transmission line. So by measuring the reflection and the transmission effects, the distance could be determined. The value of effective dielectric constant, ε_e which is 1, and the characteristic impedance Z_0 that is preset at 50Ω are substituted in (11) and (12) keeping a fixed channel height *b*, say 200μm. The *w/b* ratio is 4.9 for the given values of Z_0 and *b*. The width of the gold line *w* obtained from the *w/b* ratio that is equal to 983μm. Length of the gold line is also an important parameter to deduce since the reflection coefficient depends heavily on it.

The idea is to obtain the reflection coefficient equal to zero, which is possible only in a special case where the total signal that is transmitted is completely reflected by 180° out of phase. Thus when the length is λ/2, the reflected wave which is completely out of phase, cancels out the transmitted wave and it seems that there is nothing there even though everything gets back. A large value of return loss corresponds to a small-reflected signal just as a large value for in-

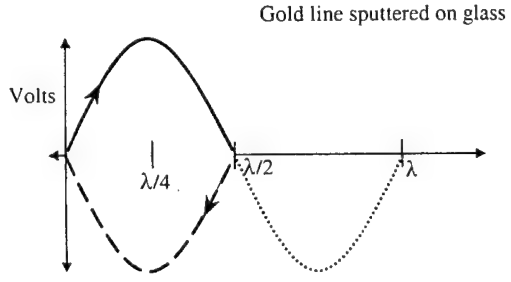

Fig. 11 Design of the transmission line (material: gold).

sertion loss corresponds to a small-transmitted signal. A marker is used to identify the frequency at which the lowest reflection coefficient is obtained. The frequency sweep/magnify feature allows zooming in a particular range of operating frequencies to obtain a much closer look at the values of the reflection coefficient.

As shown in Fig. 11, the length could be anything that satisfies the relation $l = \lambda/2 + n$, where n is a positive integer. The condition of obtaining $\Gamma = 0$ is satisfied for all values of l as far as it satisfies the given relation. The length is fixed to $\lambda/2$ in this case because of the restraints from the machine which is used for depositing gold on the glass plate. The maximum length of the glass that the machine can handle is 11.4 cm in length. So the glass cover plate was separated into two pieces with one piece of length 10.16 cm. The exact design of the gold line is shown in Fig. 8. The average length of the gold line is obtained by taking the mean of the inside line and outside line. This length is 321.29mm. The operating frequency is obtained from the relation, $c = \lambda f$; where $\lambda = 2l$. The frequency thus obtained is 466.867 MHz. Since the range of the operating frequencies for the HP 4395A is 10KHz ~ 500 MHz, the maximum wavelength λ is limited to 600mm. This is the reason for the curved shape of the gold line, rather than a straight line, which will have reduced losses. The higher the operating frequency, the shorter the length of the transmission line and better the reflection characteristics.

Figs. 12 and 13 are the screen-shots taken from the Network Analyzer HP4395A display screen showing a minimum reflection occurring at 458.5 MHz and 456.7 MHz respectively. The reflection coefficient of the transmission line for the given designed parameters should be equal to zero in an ideal case, but there are return losses for the reasons mentioned below.

1. The gold line as shown in Fig. 8 has got three curves that contribute erratic reflection of the signal in unwanted directions.
2. The launching of the co-axial from the HP 4395A to the gold line involved a mechanism, which made a compressed fit between the co-axial and the line. This method of launching the co-axial scrapes away some percent of the line at every attempt to make a connection. Furthermore, at least 8 to 10 such attempts are required for successful connections to take a complete set of data for a particular channel height.
3. Low interference of the electromagnetic waves is caused due to the metalization on the sensor, which is placed exactly on the bottom side of the gold line with its face towards the line and is separated by the distance of the channel height.
4. The width of the gold line is not constant throughout the entire length as shown in Fig. 8. Instead, there are variations in the width at quite a few places. The width was then made constant by manual scraping of the gold with a sharp blade. Such varying width causes reflection losses.

These reasons attribute toward a non–zero value of the reflection coefficient and the results drift by extremely small values as return losses. So the channel height needs to be backtracked from the obtained value of

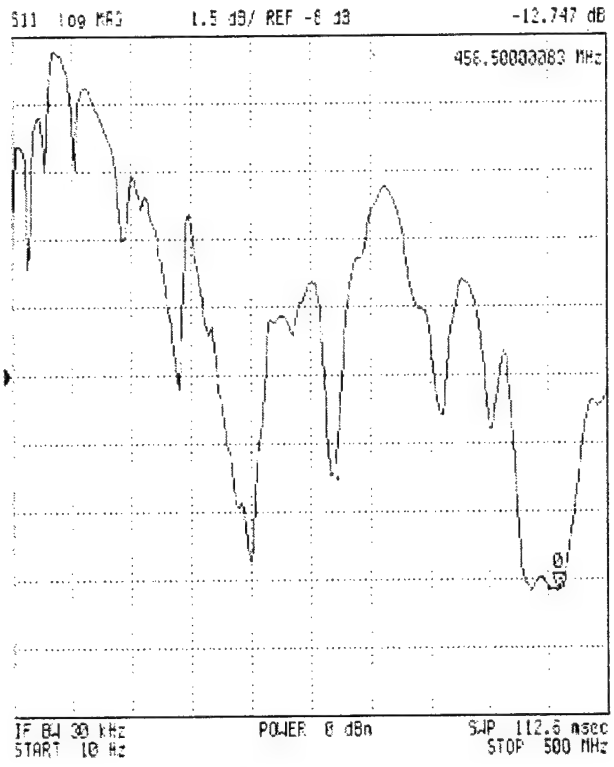

Fig. 12 Network analyzer plot showing minimum reflection at 458.5 MHz.

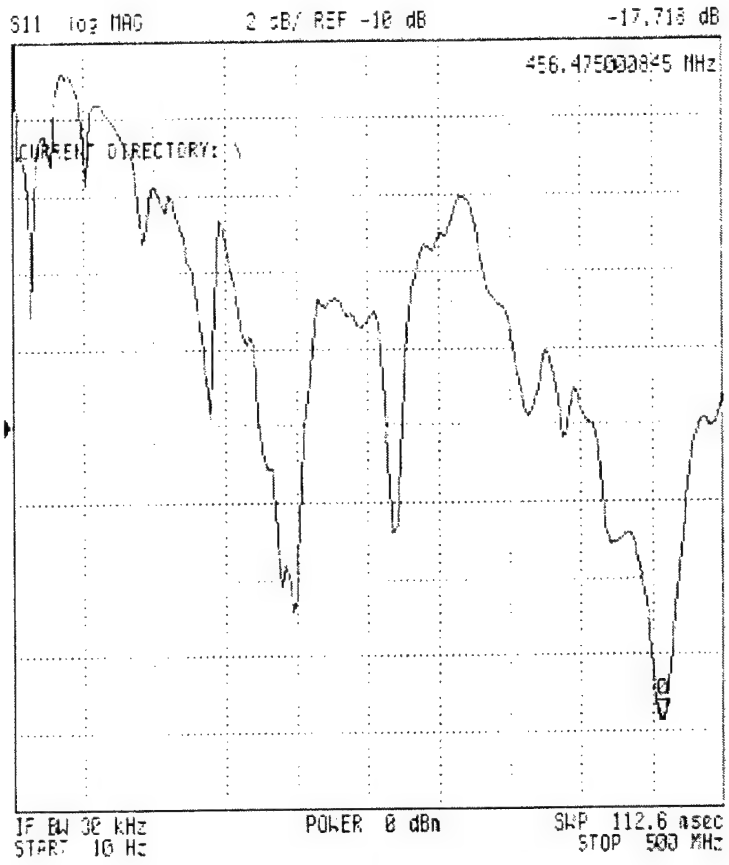

Fig. 13 Network analyzer plot showing minimum reflection at 456.47 MHz.

return losses. The reflection coefficient is obtained in dB (decibels) from the HP 4395A. These values are then used to obtain the reflection coefficient Γ. Ref. 19 details the theory and the equations that were used for obtaining the reflection coefficient Γ. The plots from the network analyzer are also shown at the end. The output from the network analyzer is obtained as return losses from which the values of Γ are calculated.

From Appendix A, the estimate for the uncertainty in the measurement of channel height is ±1.5%.

B. PRESSURE GRADIENT

The negative pressure gradient $\frac{dp}{dx}$ along the flow path is characterized with the help of a pressure transducer OMEGA® PX236 that is connected to five pressure taps, which are evenly located inside the flow channel. The pressure transducer is calibrated according to the NIST standards and procedures. A common switch is used to connect the pressure transducer to each of the five pressure taps; thus eliminating the need of more pressure sensors. Once the pressure readings are obtained, the dynamic property of the flow can be inferred from the plot of the pressure gradient. A fifth order

polynomial curve fit $p(x) = ax^5 + bx^4 + cx^3 + dx^2 + ex + f$ is then made to these pressure data to obtain the pressure at the sensor location x. The pressure gradient

$$p'(x) = 5ax^4 + 4bx^3 + 3cx^2 + 2dx + e$$

at the sensor location 'x' is obtained from interpolation of the curve. The estimated uncertainty of pressure gradient determination for the presented work is ±0.2%.

C. MACH NUMBER

Mach number is determined after measuring the average fluid velocity at the sensor location V_{sensor}. V_{sensor} is a function of the volumetric flow rate 'Q_{sensor}' and the cross sectional area 'A' of the fluid flow.

$$V_{sensor} = \frac{Q_{sensor}}{A}$$

The flow rate Q_{sensor} at the sensor location is determined from the measurements taken upstream of the channel by a NIST calibrated variable area flowmeter. The scale of the rotameter is calibrated on the assumption that its output is at atmospheric pressure, which actually is subjected to back pressure. This pressure force pushes the rotameter float to slide down the scale, resulting in a measurement that is lower than the actual flow rate Q_{rot}. To eliminate this small error in the measurement of the flow rate, a simple correction factor can be determined for differing back-pressures.[22] Assuming isothermal flow, if pressure at the exit of the rotameter, P_{rot} is measured, for a given flow rate reading, Q_{rot}, the flow rate at the sensor location, Q_{sensor} is given by,

$$Q_{sensor} = Q_{rot} \frac{\sqrt{P_{rot} P_{atm}}}{P_{sensor}}$$

where, P_{sensor} is the pressure at the location of the sensor and P_{atm} is atmospheric pressure. The velocity at the sensor location is then measured by dividing the actual flow rate at the sensor location, Q_{sensor}, by the cross-sectional area under through the fluid flows.

$$V_{sensor} = \frac{Q_{sensor}}{A}$$

Mach number is then determined by comparing the sensor velocity to the local speed of sound , V_{sound} at the measured temperature.

$$M = \frac{V_{sensor}}{V_{sound}}$$

The Mach number where choking occurs for an isothermal flow of a perfect gas in a constant duct area in the presence of wall friction is given by $1/\sqrt{\gamma}$.[23]

D. Thickness and Gap Measurements

The values of the thickness of the floating element 't' and the gap spacing between the floating element and the fixed substrate 'g' are obtained from the actual design specifications of the floating element. The values of 'g' and 't' are 0.0025 mm and 0.0020 mm respectively. Even a 10% variation from design values of 't' and 'g' contribute negligibly to the error in 'τ_w' measurements.

VII-A. Calibration Flow Channel Test Results

Two sets of tests were run. In the first, the channel was run without a sensor in place. In the second set, a sensor was installed and calibration run implemented.

Initial experiments on the flow channel were performed without the shear stress sensor in place and were aimed at ascertaining the flow channel performance and capabilities. The pressure readings along with the Mach number determinations were com-

pared with the theoretical values for a steady one-dimensional isothermal flow with friction in a constant-area duct. The well-known phenomenon of choking, the limiting condition for such a flow in a constant-area duct, is also observed with the present calibration flow channel.

Fig.14 shows the nearly variation of Mach number with increase in the flow rate inside the flow channel at channel height 230 μm. Mach 0.40 was obtained at a flow rate of 43960 sccm at a channel height of 230 μm. As the flow rate increases, the shear stress at the location of the sensor element increases in a monotonic fashion as shown in Fig. 15.

As the gas flows along the flow channel, its static pressure decreases. Eventually a limiting condition is reached where the length of the pipe cannot be increased without altering the upstream conditions; that is, the flow has choked. At that point, *dx/dp* is equal to zero. The limiting or choking Mach number for steady one-dimensional isothermal flow with friction in a constant- area duct is $M=1/\sqrt{\gamma}$. Thus, for $\gamma=1.4$, the theoretical choking Mach number (at the channel exit) is 0.845. At choking the shear stress at the sensor location is 80.55 Pa, and the Mach number at the sensor location is 0.40.

Fig. 14 shows the Mach number distribution along the flow channel at the channel height of 230 μm. The distance from the point where the sensor is located inside the channel bed to the exit of the channel is 16.9 mm. At limiting conditions for a steady one-dimensional isothermal flow with friction in a constant-area duct, the equation relating

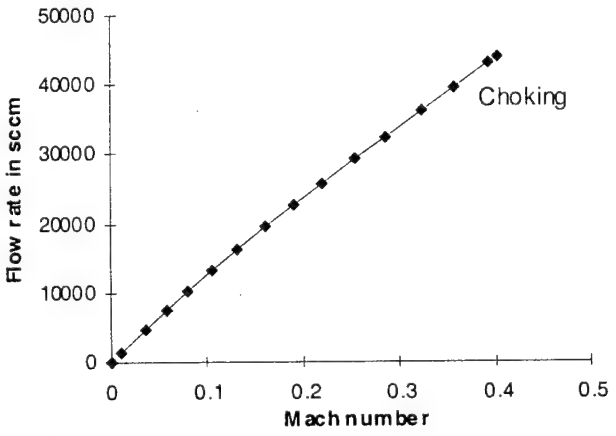

Fig. 14 Mach number at sensor location as a function of flow rate inside the calibration flow channel.

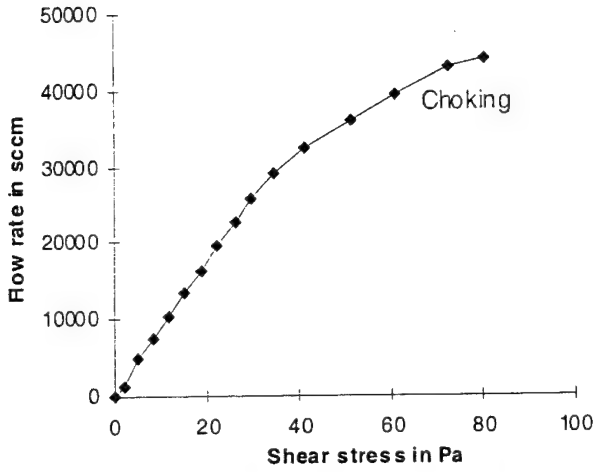

Fig. 15 Shear stress variation with increase in flow rate in the calibration channel.

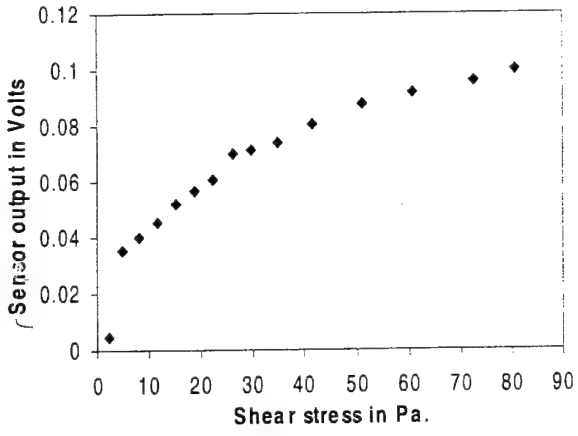

Fig. 16 Typical response of CWRU/Analog Devices MEMS shear stress sensor at channel height of 230 μm (sensor-1).

the friction term '$4fL_{max}/D$' and the inlet Mach number M is,

$$\frac{4fL_{max}}{D} = \frac{1-\gamma M^2}{\gamma M^2} + \ln(\gamma M^2)$$

where, f is the friction factor $\left[f = \frac{\tau}{1/2\rho V^2}\right]$, γ is the ratio of specific heats of compressed nitrogen at 23°C, D is the hydraulic diameter of the channel [D = 2 x channel height] and L_{max} is the length to choking in the channel from the station where the local Mach number is M. Any increase in the length would then alter the upstream conditions. The Mach number at the sensor location implies a value of $4fL_{max}/D$ for choking. For M = 0.40, $4fL_{max}/D$ = 1.9682. At choking, the shear stress at that sensor location is 80.5 Pa. The friction factor f is 0.0124. For L_{max} = 16.9 mm and D = 0.460 mm, $4fL_{max}/D$ = 1.84. This is in close agreement to the theoretical value of 1.9682.

VII-B. MEMS Shear Stress Sensor Calibration Results

A typical MEMS shear stress sensor fabricated at Advanced MicroMachines for Industry (AMMI), now a part of BF Goodrich, and packaged at Case Western Reserve University is mounted inside the flow channel

for calibration. The shear stress values at different flow rates for a fixed channel height are obtained and shear stress data versus output voltage is plotted. Figs. 16 and 17 show the measured output of the multimeter versus the shear stress for two different sensors of similar design at the channel heights of 230 μm and 265 μm respectively.

In Fig. 16, an irregularity in the curve is observed for a small portion of the plotted data before the response behaves in a linear fashion. This is due to the stiction effect. The plot shows two regimes with a different sensitivity where the sensor behaves linearly. The sensitivity of the sensor, at 230 μm channel height, in the regime I (up to ~ 25 Pa) is 1.604 mV/Pa and in the regime II (beyond 25 Pa) is 0.57 mV/Pa. The linear response for regime I is in the 0.03 V ~ 0.06 V range and in the 0.065 V ~ 0.1 V range for regime II. The calibration accuracy is ±2% (see Appendix A).

Similar response in the output is observed in a second sensor calibration for the channel height of 265 μm. Fig. 17 is the plot of shear stress versus output voltage for the calibrated sensor a channel height of 265 μm. In regime I (up to ~ 25 Pa), the shear stress sensor exhibits a sensitivity of about 0.08 mV/Pa in the linear operating range of 0.5 mV to 2.5 mV, while in the regime II (beyond 25 Pa), the sensitivity of 0.023 mV/Pa in the linear operating range of 2.5 mV to 4 mV is observed. The calibration accuracy again is within 2%.

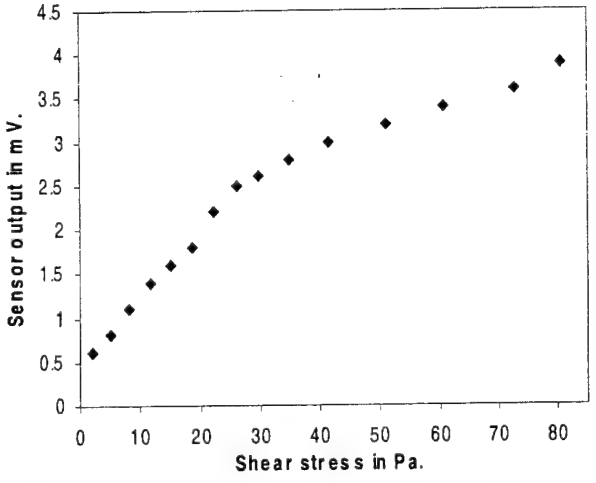

Fig. 17 Typical response of CWRU/Analog Devices MEMS shear stress sensor for channel height of 265μm (sensor-2).

It is interesting to observe the similarity in the transition from regime I to regime II in the output of both the sensors that were calibrated. The change in the sensors sensitivity starts when the shear stress value reaches 26 Pa at the sensor location and continues till the shear stress reaches 32 Pa at the sensor location. The sensitivities of both the sensors at different channel heights locations remains constant below the shear stress value of 26 Pa (regime I) and also above 32 Pa (regime II).

The reason behind this change in sensitivity is attributed to the actual floating element design on the sensor chip. In regime I, the sensor is operating completely in a forced-balanced mode. The sensor element is in its null position and the supporting beams are not deflected. In regime II, the floating element begins to displace so that part of the restoring force is borne by the beams while the rest by the capacitive restoring force. This explains the reduced sensitivity in regime II. Since both the beam deflection and capacitive restoration are linear, the response in regime II remains linear but with reduced sensitivity.

There is a noticeable jump in the output of Fig. 16 from 0.005 V to 0.035 V. This jump is the effect of stiction, a typical problem frequently encountered in the microfabrication of microelectromechanical structures.

The microstructure, floating element in the present case, will be stuck to the substrate or electrostatically shield immediately beneath the surface. At very low flow rates, the shear force produced by the fluid flow is not sufficient to overcome the stictional forces beneath the surface. With the increase in the flow rate, a finite shear force that is required to overcome this stictional force is generated and the sensor element, which is the floating element in this case, frees itself from the substrate. Once this has occurred and the shear forces dominate the stiction

forces, the floating element deflects in a linear manner.

This problem could be rectified with the help of a microcontroller integrated on the same chip. Erasable Programmable Read Only Memory 'EPROM' stores the offset coefficient and the microcontroller makes the accurate corrections so that all the sensors with the same specification exhibit similar output properties when subject to similar input conditions. The sensors at Analog Devices Inc. undergo a process called 'Laser Trimming of Resonant Structures' which normalizes the output of all the sensors to a standard output. This takes cares of the varying offset value in different sensors of the same kind. With the design package, some faltering is caused in the output of the sensor occasionally due to the imperfections and the breaks in the gold line that is brought out of the channel from the sensor pads for external connections. This problem can be rectified by an enhanced masking process or by thickening the gold line to 8000 A°. The present thickness of the gold line is 5000 A°.

It has also been observed that the sensor shows photosensitive characteristics. Illumination causes drifts and wavering in the output voltage on the order of several microvolts. Fluctuations in the signal caused primarily by noise, rotameter drift, illumination and measurement circuit was detected by data acquisition instruments and read outs from these instruments were corrected by changing the offset value before analyzing the collected data.

When the flow is initiated at the start of the experiment by opening of the rotameter valve, a transient increase of a few hundred milli-volts in the output signal is observed. It has a characteristic decay time of approximately 30-35 seconds. After the decay, the output stabilizes itself to a steady drift, which is then considered as the offset value for the multimeter and is thereupon included

as a correction term. This steady drift is considered to be the fixed error for the particular experimental run and is repeatable. Repeatability can be verified by obtaining the same range of the drift after closing and opening the valve of the rotameter.

Saturation of the circuit is obtained at higher shear stresses because the circuit cannot generate strong enough electrostatic forces to counter the shear forces caused by the fluid flow. Saturation level is subject to sensor sensitivity variation, which is inevitable even between mountings and positioning of the same sensor.

VIII. Uncertainty Analysis

Uncertainty analysis refers to a process of estimating how great an effect the uncertainties in the individual measurements have on the calculated result. The square-root-of-the-sum-of-the-squares method, as described by Moffat, is used for computing an absolute error of the uncertainties that are incorporated with the calibration.[24] In this method, the relative weight of each measurement is taken into consideration as a linear operator based on its power relationship to the value. First, the fractional uncertainties of the individual variables that are used in the calibration equation are measured. Then, the partial derivative of the equation is taken with respect to each component and divided by the total to obtain an equation for how the fractional uncertainties compound. Thus, the fractional uncertainty $\Delta\tau/\tau$, which is also defined as the fractional uncertainty of the calculated effective stress, can be calculated from (9)

$$\frac{\Delta\tau_{eff}}{\tau_{eff}} = \left[\sum\left(\frac{\partial\tau_{eff}}{\partial X_i}\Delta X_i\right)^2\right]$$

Applying the square root of the sum of the squares rule to (9), the fractional uncertainties of the individual quantities can be obtained;

$$\frac{\Delta\tau_{eff}}{\partial\left(\frac{\partial p}{\partial x}\right)} = -\frac{\tau_{eff}}{\left(\frac{\partial p}{\partial x}\right)}$$

$$\frac{\Delta\tau_{eff}}{\partial(b)} = -\frac{\tau_{eff}}{(b)}$$

$$\frac{\Delta\tau_{eff}}{\partial M} = -\left(\frac{\partial p}{\partial x}\right)\left(\frac{b}{2}\right)(-2\gamma M) = \frac{-2\gamma M\tau_{eff}}{\left[1-\gamma M^2+\frac{g}{b}+\frac{2t}{b}\right]}$$

$$\frac{\Delta\tau_{eff}}{\partial g} = -\left(\frac{\partial p}{\partial x}\right)\left(\frac{b}{2}\right)\left(\frac{1}{b}\right) = \frac{\left(1/b\right)\tau_{eff}}{\left[1-\gamma M^2+\frac{g}{b}+\frac{2t}{b}\right]}$$

$$\frac{\Delta\tau_{eff}}{\partial t} = -\left(\frac{\partial p}{\partial x}\right)\left(\frac{b}{2}\right)\left(\frac{2}{b}\right) = \frac{\left(2/b\right)\tau_{eff}}{\left[1-\gamma M^2+\frac{g}{b}+\frac{2t}{b}\right]}$$

Therefore combining all individual uncertainties, we get the fractional uncertainty of the calculated effective shear stress[‡];

$$\left(\frac{\Delta\tau_{eff}}{\tau_{eff}}\right)^2 = \left(\frac{\Delta\frac{\partial p}{\partial x}}{\frac{\partial p}{\partial x}}\right)^2 + \left(\frac{\Delta b}{b}\right)^2 +$$

$$\left(\frac{2\gamma M\Delta M}{\left[1-\gamma M^2+\frac{g}{b}+\frac{2t}{b}\right]}\right)^2 + \left(\frac{\left(1/b\right)\Delta g}{\left[1-\gamma M^2+\frac{g}{b}+\frac{2t}{b}\right]}\right)^2$$

$$+\left(\frac{2\Delta t/b}{\left[1-\gamma M^2+\frac{g}{b}+\frac{2t}{b}\right]}\right)^2 \qquad (13)$$

Each term represents the contribution made by the uncertainty in one factor to the overall uncertainty in the result.

Taylor presents a systematic approach to the identification and estimation of measuring system errors based on manufacturer's specifications.[25] The instruments that are used in the calibration process are pressure transducer, rotameter, network analyzer and multimeters. Rotameter, for the measurement of Mach number at the sensor location;

[‡] The terms inside the sets of parentheses are the fractional uncertainties of the individual quantities.

Pressure transducer, to calculate the pressure gradient along the channel length, Network Analyzer, to measure the channel height and multimeters are used for digital/analog data acquisition.

The transducer calibration was found to be very well within 1% accuracy as specified on the calibration sheet. The inaccuracies of the pressure sensor from the taps contribute in a non-linear fashion since the gradient is the derivative of a line based on a measured distance. If the pressures for the curve fit are modified by +1% at the maximum and -1% at the minimum value, corresponding to the modified deviance in the pressure gradient, the pressure at the location of the sensor changes less than 0.2%.

Thus, maximum calculated $\left(\frac{\Delta \frac{\partial p}{\partial x}}{\frac{\partial p}{\partial x}} \right) = 0.002.$

Due to the tendency of the rotameter to drift during a constant flow, the volumetric flow rate varies and leads to uncertainty. This would lead to a slightly different pressure reading due to the varying flowrates and the sensor output would not correlate to the recorded flowrate and pressure gradient. To avoid this uncertainty, a different rotameter with a higher range from the original one was used and run at the same flowrates for the same test conditions. The pressure gradient and the sensor output are comparable to the one obtained from the original rotameter. Uncertainty contributed from this drift is typically on the order of 5 to 10%.

The relationship of the uncertainty in the Mach number factor to that of the total compressibility correction is obtained by taking the derivative of the correction factor. The compressibility correction is less than 0.1% at low shear stresses yielding the compressibility correction fractional uncertainty less than 0.1%. The maximum compressibility correction fractional uncertainty (~ 0.5%) occurs at higher shear stresses where M=0.40. If the inaccuracies in the channel

height measurement and the pressure gradient measurements are reduced to the level comparable to that needed for 1% calibration accuracy, the uncertainty in the compressibility correction drops due to the dependence on channel height uncertainty in its calculation. Thus, the uncertainty in the compressibility correction factor can be neglected for any flowrate, any shim, and any reasonable accuracy limits of calibration. The fractional uncertainties of the underflow shear stresses are neglected following the same line of reasoning. The maximum uncertainty in the measurement of the Mach number $\left(\frac{\Delta M}{M}\right)$ is 0.025.

Measurements done using the new technique indicate a sensitivity of about ± 3μm, which is about ±1.5% for a channel height of 200 μm. Also, the maximum uncertainty in the measurement of 'g', the gap spacing between the floating element and the fixed substrate $\left(\frac{\Delta g}{g}\right)$ and 't', the thickness of the floating element $\left(\frac{\Delta t}{t}\right)$ is 0.1. These had negligible effect on overall error.

For,

$$\left(\Delta\frac{\frac{\partial p}{\partial x}}{\frac{\partial p}{\partial x}}\right)=0.002,\ \left(\frac{\Delta g}{g}\right)=0.01,\ \left(\frac{\Delta t}{t}\right)=0.01,$$

$$\left(\frac{\Delta b}{b}\right)=0.015, \text{ and } \Delta M=0.0$$

Therefore from (13), the total uncertainty of the effective wall shear stress $\left(\frac{\Delta\tau_{eff}}{\tau_{eff}}\right)$=0.02 at M=0.4 and 0.015 at M=0. Thus, MEMS shear stress sensors are calibrated to an uncertainty of ±2%. The last 3 terms obtained as the uncertainties from the measurement of Mach number, the gap between the floating element and the fixed substrate and the thickness of the floating element are negligible and are not considered as a major source of uncertainty. The measurements of the channel height and the

pressure gradient are considered to be the largest sources of error and are a major contribution of uncertainty towards the overall uncertainty of the effective wall shear stress.

IX. Summary and Conclusion

A calibration flow channel and a calibration procedure based on continuum isothermal constant-area compressible channel flow have been developed. The calibration channel capabilities have been greatly increased and are now able to sustain shear stresses to 80 Pascal. The response of the sensor was studied as a function of flow rate and the channel height. A novel microstrip technique that was implemented for measuring channel height was successful in reducing the inaccuracy from ±20 μm to ±3 μm. MEMS wall-shear-stress sensors incorporating the floating element technique with integrated electronics have been successfully calibrated with an accuracy of ±2%.

Acknowledgments

This work was supported by the Air Force Office of Scientific Research under contract AFOSR grant F49620-96-1-0482. Authors would also like to thank Microfabrication Laboratory staff and Electronics Design Center staff at Case Western Reserve University for their support. Special thank goes to Dr. Daniel Hyman, Dr. Avijit Bhunia and Pranjal Pathak for providing their expertise and interest in MEMS shear stress sensors calibration research.

References

[1] H. Alfredsson and A. Johansson, The Fluctuating Wall-Shear Stress and the Velocity field in the Viscous sub-layer, *Phys. Fluids,31* (1988) 1026-1033.

[2] J. Preston, The Determination of Turbulent Skin Friction by means of Pitot tubes, *J. Roy. Aero. Soc.*, 58 (1954) 109-121.

[3] K. G. Winter, "An Outline of the Techniques Available for the Measurement of Skin Friction in Turbulent Boundary Layers," *Progress in Aerospace Sciences* Vol.18 (1977), pp. 1-57.

[4] M. Sheplak, E. Spina and C. McGinley, The Application of Hot-Film Anemometry to Hypersonic Flow, *25th Alaa Fluid Dynamics Conference, Colorodo Springs, USA, June 20-23, 1994.*

[5] Pan, T., Hyman, D., Mehregany, M., Reshotko, E., and Garverick, S., "Microfabricated Shear Stress Sensors, Part I: Design and Fabrication," AIAA Journal, Vol. 37, No. 1, 1999, pp. 66-72.

[6] Hyman, D., Pan, T., Reshotko, E., and Mehregany, M., "Microfabricated Shear Stress Sensors, Part II: Testing and Calibration," AIAA Journal, Vol. 37, No. 1, 1999, pp. 73-78.

[7] T. Pan, "Microfabricated Shear Stress Sensors," *Ph.D. Thesis*, Case Western Reserve University, January, 1996.

[8] Daniel J. Hyman, "Testing and Calibration of MicroFabricated Shear Stress Sensors," *M.S. Thesis*, Case Western Reserve University, May 1996.

[9] Patel, M., "Development of MEMS Wall Shear Stress Calibration System," M.S. Thesis, Dept. of Mechanical and Aerospace Engineering, Case Western Reserve University, Cleveland, OH, May 2000.

[10] W. C. Tang, T. H. Nguyen, and R. T. Howe, "Laterally Driven Polysilicon Resonant Microstructures," Sensors and Actuators, Vol 20 (1989), pp. 25-32.

[11] W. C. Tang, T. H. Nyugen, M. W. Judy, and R. T. Howe, "Electrostatic comb Drive of Lateral Polysilicon Resonators," Sensors and Actuators, Vol21-23 (1990), pp. 328-331.

[12] W. C. Tang, "Electrostatic Comb Drive for Resonant Sensor and Actuator Applications," Ph.D. Thesis, University of California at Berkley, 1990.

[13] M. A. Schmidt, R. T. Howe, and S. D. Senturia, "A Micromachined Floating-element Shear Stress Sensor", *The 4th International Conference on Solid-State Sensors and Actuators,* Tokyo, Japan, 1987, pp. 383-386.

[14] M. A. Schmidt, R. T. Howe, S. D. Senturia, and J. H. Haritonidis, "Design and Calibration of a Microfabricated Floating-element Shear Stress Sensor", *IEEE Trans. Elecron Devices,* Vol. 35, June 1998, pp. 750-757.

[15] M. A. Schmidt, "Microsensors for the Measurement of Shear Forces in Turbulent Boundary Layers", *Ph.D. Thesis*, Massachusetts Institute of Technology, 1988.

[16] T. Hanratty and J. Campbell, in R. Goldstein (ed.), Measurement of Wall Shear *Stress in Fluid Mechanics Measurements*, Hemisphere, New York, 1983, p. 559-615.

[17] T. A. Core, W. K. Tsang, and S. J. Sherman, " Fabrication Technology for an Integrated Surface-Micromachined Sensor,: Solid State Technology, Oct., 1993, pp. 39-47.

[18] W. Kuenel and S. J. Sherman, "A Surface Micromachined Silicon Accelerometer with On-Chip Detection Circuitry," Sensors and Actuators, A 45, 1994, pp. 39-47.

[19] David M. Pozar, University of Massachusetts at Amherst, "*Microwave Engineering*", John Wiley & Sons, Inc.

[20] Laurie A. Dudik, C.C. Liu, "Thick Film Screen Making", *Standard Operating Procedure for thick Film Screen Making*, Case Western Reserve University, June 12, 1996.

[21] Laurie A. Dudik, C.C. Liu, "Screen Printing on Inks on Substrates", *Standard Operating Procedure for thick Film Screen Making*, Case Western Reserve University, June 12, 1996.

[22] E. O. Doeblin, *Measurement Systems*, 4th ed., McGraw Hill, 1990, pp. 576-577.

[23] Maurice J. Zucrow, Joe D. Hoffman, *Gas Dynamics*, Vol.1, John Wiley and Sons, Inc., pp. 272-275.

[24] Robert J. Moffat, Describing the Uncertainties in Experimental Results, *Experimental Thermal and Fluid Science*, 1:3-171988.

[25] Taylor, J. L., Computer-Based Data Acquisition Systems: Design Techniques, *Instrument Society of America*, 1986.